Monthly Notices
of the
ROYAL ASTRONOMICAL SOCIETY

Mon. Not. R. Astron. Soc. **403,** 1993–1998 (2010) doi:10.1111/j.1365-2966.2009.16228.x

Effect of plasma composition on the interpretation of Faraday rotation

Kiwan Park★ and E. G. Blackman★

Department of Physics and Astronomy, University of Rochester, Rochester, NY 14627, USA

Accepted 2009 December 17. Received 2009 December 14; in original form 2009 August 25

ABSTRACT

Faraday rotation (FR) is widely used to infer the orientation and strength of magnetic fields in astrophysical plasmas. We first derive exact expressions of FR that are more general than the previous work in allowing for a plasma of arbitrary composition, arbitrary net charge and arbitrary radiation frequency. The latter includes low-frequency regimes where resonances occur and FR changes sign. We then show how the expressions can be used to constrain degeneracies between plasma density, composition and inferred magnetic field strength in astrophysically relevant ion–electron–positron plasmas of unknown positron to electron number density ratio. Electron–positron pairs may be prevalent in the plasma magnetospheres of pulsars, black holes and active galactic nuclei (AGN) jets, but the fraction of positive charge carriers that are protons or positrons has been difficult to determine. FR is sensitive to the plasma composition which may be helpful. A pure neutral electron–positron plasma has negligible FR, and the greater the fraction of positrons the higher the magnetic field strength required to account for the same FR. We consider parameters relevant to AGN jets and clusters to show the degeneracies in field strengths and plasma composition for a given FR measured value as a function of the plasma composition. We point out that these results can be used to constrain the plasma composition if an independent measurement of the magnetic field strength can be combined with the FR measure.

Key words: magnetic fields – plasmas – methods: analytical – ISM: magnetic fields – galaxies: jets – radio continuum: general.

1 INTRODUCTION

Faraday rotation (FR) describes the effect by which the electric field vector of propagating electromagnetic (EM) radiation rotates as it propagates through a magnetized plasma. The EM waves interact with charged particles such that left-handed circularly polarized (LHP) and right-handed circularly polarized (RHP) waves experience different refractive indices and propagate at different phase velocities. The net electric field vector rotates as the wave propagates. The total FR between source and observer depends on the strength and orientation of the intervening magnetic field along the line of sight, the plasma density and the plasma composition. FR has been used, for example, to constrain the strength, gradient and direction of magnetic field in active galactic nuclei (AGN) jets (Asada et al. 2002, 2008; Attridge, Wardle & Homan 2005; Zavala & Taylor 2005), galaxy clusters (e.g. Kim et al. 1990) and the galactic intersteller medium (ISM; e.g. Han et al. 2006).

Typically, FR is calculated for a neutral ion–electron plasma. While this is a good approximation for the plasma of the galactic ISM and galaxy clusters, it is less reliable for magnetospheres and outflows around neutron stars and black holes. In particular, constraining the composition of jets in AGN is observationally difficult because only the electrons or positrons radiate efficiently, so free energy in protons is hard to detect directly. The plausible predominance of electron plasma in the magnetosphere of the black hole and the uncertainty as to whether jets emanate directly from its magnetosphere (Blandford & Znajek 1977) or from the surrounding accretion disc (Livio, Ogilvie & Pringle 1999) has contributed in making the composition determination a long standing puzzle. The basic question of how far a jet would be force free (Li et al. 2006) is also a fundamental issue. Indirect theoretical constraints on AGN jet plasma composition reach to mixed conclusions: Celotti & Fabian (1993) and Ghisellini (2008) favour predominately electron–proton jets, whilst Reynolds et al. (1996) favour a predominantly electron–positron jet for M87. Hubbard & Blackman (2006) argued that on the largest scales, stellar wind mass loading will significantly proton load the jet regardless of its initial composition. It is therefore important to identify possible new techniques for determining jet plasma composition and to be aware of its effect on measurements such as FR.

With the above motivations in mind, we first derive a general expression for FR that incorporates arbitrary plasma composition for arbitrary radiation frequency range in Section 2. We discuss how this is more general than previous expressions. In Section 3,

★E-mail: pkiwan@pas.rochester.edu (KP); blackman@pas.rochester.edu (EGB)

we then focus on a neutral ion–electron–positron plasma and show how a fixed FR leaves degeneracies in the magnetic field and electron density for different values of the electron to positron number density ratio. We discuss a strategy for how these degeneracies can in principle be used to constrain the plasma composition in AGN jets when an independent measure of the magnetic field strength can be obtained. We conclude in Section 4.

2 GENERALIZED FARADAY ROTATION

2.1 Formalism for arbitrary neutral plasmas

To formally derive FR for an arbitrary neutral plasma, we assume a cold neutral plasma in a background external magnetic field $\boldsymbol{B}_{\rm ex}$, subject to a perturbation from a propagating EM wave. [The cold plasma approximation for FR has been shown to be effective for the electron contribution to FR even for quasi-relativistic plasmas (Skilling 1971), and we discuss this further below equation 16]. For the electric field $\boldsymbol{E}$, magnetic field $\boldsymbol{B}$ and induced particle velocity $\boldsymbol{v}_s$ (where the index s indicates particle species), we write

$$\begin{aligned}\boldsymbol{E} &= \boldsymbol{E}_1,\\ \boldsymbol{B} &= \boldsymbol{B}_1 + \boldsymbol{B}_{\rm ex},\\ \boldsymbol{v}_s &= \boldsymbol{v}_{s1},\end{aligned} \tag{1}$$

where $\boldsymbol{E}_1$ and $\boldsymbol{B}_1$ are perturbations such that $|B_1/B_{\rm ex}| \ll 1$, $|E_1/B_{\rm ex}| \ll 1$ and $|v_{s1}| \ll c$. We also assume a neutral plasma so that

$$\sum_s n_{s0} e_s = 0, \tag{2}$$

where n_{s0} is the unperturbed density of a particle of species s, and e_s is charge of particle of species s.

Using the above formalism, Maxwell equations become (e.g. Gurnett & Bhattacharjee 2005)

$$\nabla \times \boldsymbol{E_1} = -\frac{1}{c}\frac{\partial \boldsymbol{B_1}}{\partial t}, \quad \nabla \times \boldsymbol{B_1} = \frac{4\pi}{c}\boldsymbol{J} + \frac{1}{c}\frac{\partial \boldsymbol{E_1}}{\partial t}. \tag{3}$$

If the current density $\boldsymbol{J} \equiv \sum_s n_{s0} e_s \boldsymbol{v}_{s1} = 0$, then E_1 and B_1 solve the plane wave vacuum equations. However, a finite $\boldsymbol{J}$ and the Lorentz force equation

$$m_s \frac{{\rm d}\boldsymbol{v}_s}{{\rm d}t} = e_s\left(\boldsymbol{E}_1 + \frac{1}{c}\boldsymbol{v}_s \times \boldsymbol{B}_{\rm ex}\right) \tag{4}$$

imply that, in general, $\boldsymbol{E}$, $\boldsymbol{B}$ and $\boldsymbol{v}_s$ are all coupled.

To quantify the interaction between the particles and EM fields, we take $\boldsymbol{v}_s$, $\boldsymbol{E}_1 \propto e^{i(\boldsymbol{k}\cdot\boldsymbol{x}-\omega t)}$ so equation (4) becomes

$$\boldsymbol{v}_s = \frac{i e_s}{m_s \omega}\left(\boldsymbol{E}_1 + \frac{\boldsymbol{v}_s}{c} \times \boldsymbol{B}_{\rm ex}\right) = \frac{i e_s}{m_s \omega}\left(\boldsymbol{E}_1 + \frac{\boldsymbol{v}_s}{c} \times \frac{m_s c\, \boldsymbol{\omega}_{cs}}{e_s}\right), \tag{5}$$

where $\omega_{cs} = e_s B_{\rm ex}/m_s c$ is the cyclotron frequency of species s. The current density can then be expressed as the product of a conductivity tensor and the $\boldsymbol{E}_1$ field, namely $\boldsymbol{J} = \boldsymbol{\sigma} \cdot \boldsymbol{E}_1$, where the conductivity tensor is given by (Ashok 2004)

$$\sigma_{ij} = \sum_s \frac{i\, n_{s0} e_s^2}{m_s \omega [1 - (\omega_{cs}/\omega)^2]}\left(\delta_{ij} - \frac{\omega_{cs,i}\omega_{cs,j}}{\omega^2} - \frac{i}{\omega}\epsilon_{ijk}\omega_{cs,k}\right). \tag{6}$$

We now take $\boldsymbol{B}_{\rm ex} = (0,\, 0,\, B)$ so that the components of equation (5) become

$$\begin{aligned}-i\omega m_s v_{sx} &= e_s\left(E_{1x} + \frac{v_{sy}}{c}B\right),\\ -i\omega m_s v_{sy} &= e_s\left(E_{1y} - \frac{v_{sx}}{c}B\right),\\ -i\omega m_s v_{sz} &= e_s E_{1z},\end{aligned} \tag{7}$$

and, the conductivity tensor becomes

$$\boldsymbol{\sigma} = \sum_s \frac{n_{s0} e_s^2}{m_s}\begin{pmatrix} \frac{-i\omega}{\omega_{cs}^2-\omega^2} & \frac{\omega_{cs}}{\omega_{cs}^2-\omega^2} & 0\\ \frac{-\omega_{cs}}{\omega_{cs}^2-\omega^2} & \frac{-i\omega}{\omega_{cs}^2-\omega^2} & 0\\ 0 & 0 & \frac{i}{\omega}\end{pmatrix}. \tag{8}$$

Equation (3) with $\nabla \rightarrow {\rm i}\boldsymbol{k}$ then becomes

$$\boldsymbol{k} \times (\boldsymbol{k} \times \boldsymbol{E}_1) + \frac{\omega^2}{c^2}\left(1 - \frac{4\pi\boldsymbol{\sigma}}{i\omega}\right) \cdot \boldsymbol{E}_1 = 0. \tag{9}$$

from which the secular equation for the FR effect is

$$\begin{pmatrix} S-\eta^2 & -iD & 0\\ iD & S-\eta^2 & 0\\ 0 & 0 & P\end{pmatrix}\begin{pmatrix} E_{1x}\\ E_{1y}\\ E_{1z}\end{pmatrix} = 0, \tag{10}$$

where $S \equiv 1 - \sum_s[\omega_{ps}^2/(\omega^2 - \omega_{cs}^2)]$, $D \equiv \sum_s\{(\omega_{cs}\omega_{ps}^2)/[\omega(\omega^2 - \omega_{cs}^2)]\}$, $P \equiv 1 - \sum_s(\omega_{ps}^2/\omega^2)$ and the plasma frequency and wave vector, parallel to $\boldsymbol{B}_{\rm ex}$ (only the component of magnetic field along photon path to the observer contributes to FR) are given respectively by $\omega_{ps}^2 = (4\pi n_s e_s^2)/m_s$ (n_s: number density) and $\boldsymbol{k} = [(\eta\,\omega)/c]\,\hat{z}$ (η: refractive index).

The solution of equation (10) for refractive index 'η' produces non-trivial FR when the two solutions for 'η' are distinct, corresponding to left- and right-handed polarization; $\eta_L^2 = S - D$, $\eta_R^2 = S + D$ with two associated $\boldsymbol{E}_1$ field eigenvectors. The transverse (x, y) components of $\boldsymbol{E}$ for each refractive index are of the same magnitude but have different phases, that is, $\boldsymbol{E}_L = (E_0, -i\,E_0, 0)$, $\boldsymbol{E}_R = (E_0, i\,E_0, 0)$, where $\pm i$ arises from the differentiation of velocity and position over time in the Lorentz force law. The equal amplitude of the transverse E field components then imply circularly polarized waves.

The different phase velocities $(c/\eta_L, c/\eta_R)$ cause the propagating LHP and RHP waves to experience a net phase angle difference when they propagate over the same distance. As a result, the net electric field phase angle $[\phi = \tan^{-1}(E_y/E_x)]$ that comes from the superposition of these handed waves rotates along the propagating distance. This is the FR. The change ϕ along the propagation distance is

$$\begin{aligned}\frac{{\rm d}\phi}{{\rm d}z} &= \frac{1}{2}(k_L - k_R)\\ &= \frac{\omega}{2c}\left[\sqrt{1 - \sum_s \frac{\omega_{ps}^2}{\omega(\omega - \omega_{cs})}} - \sqrt{1 - \sum_s \frac{\omega_{ps}^2}{\omega(\omega + \omega_{cs})}}\right].\end{aligned} \tag{11}$$

Having derived the general formalism for a neutral plasma of arbitrary composition and the exact equation for FR (equation 11), we note that Hall & Shukla (2005) considered FR in an ion–electron–positron plasma producing the approximate analytical result

$$\frac{{\rm d}\phi}{{\rm d}z} \sim Z_i n_i \frac{2\pi e^3 B}{m_e^2 c^2 \omega^2}, \tag{12}$$

where Z_i is the ion charge number. Then, equation (12) agrees with equation (11) in the high frequency limit for an ion–electron–positron plasma, a point we will return to in Section 2.3. Equation (12) indicates that there is no rotation in case of an electron–positron pair plasma ($n_i = 0$). For $n_i \neq 0$, ions generate the FR by breaking the symmetry of a pair plasma. Note however that in practice, since the electron density is the quantity usually measured, it would be better to express n_i as a function of n_e (equation 15).

2.2 Ion–electron plasma

For a pure (hydrogen) ion–electron plasma, equation (2) takes the form $n_e + n_i = 0$, where n_e and n_i are the electron and hydrogen ion number densities. The summation over s in equation (11) also involves terms corresponding to electrons and ions, respectively. However, because of the large ion to electron mass ratio $m_i/m_e = 1836$, the ion terms are typically ignored (e.g.Asada et al. 2002, 2008; Zavala & Taylor 2005). Then the rotated angle integrated along the line of sight for the distance l (e.g. Reynolds et al. 1996) becomes

$$\begin{aligned}\phi &\simeq \int_0^l \frac{\omega}{2c}\left[\sqrt{1-\frac{\omega_{pe}^2}{\omega(\omega-\omega_{ce})}}-\sqrt{1-\frac{\omega_{pe}^2}{\omega(\omega+\omega_{ce})}}\right]\cdot \mathrm{d}z,\\ &\sim \frac{2\pi e^3}{m_e^2c^2\omega^2}\int_0^l n_e B\cos\theta\ \mathrm{d}z,\\ &= \left(\frac{e^3}{2\pi m_e^2c^4}\int_0^l n_e B\cos\theta\ \mathrm{d}z\right)\cdot\lambda^2 \equiv RM\cdot\lambda^2, \end{aligned} \tag{13}$$

where the second relation follows for $\omega \gg \omega_{pe}, \omega_{ce}$. The general procedure for determining *RM* is to measure ϕ at multiple wavelengths and infer a slope of the ϕ versus λ line.

2.3 Ion–electron–positron plasma

For the hydrogen ion–electron–positron case, equation (2) becomes

$$-en_e + en_{e^+} + en_i = 0, \tag{14}$$

where n_{e^+} is the positron number density. We now define $X \equiv n_{e^+}/n_e$ so that

$$n_{e^+} = n_e X, \quad n_i = n_e(1 - n_{e^+}/n_e) = n_e(1 - X). \tag{15}$$

equation (11) then becomes

$$\begin{aligned}\frac{\mathrm{d}\phi}{\mathrm{d}z} &= \frac{\omega}{2c}\left[\sqrt{1-\frac{\omega_{pe}^2}{\omega(\omega-\omega_{ce})}-\frac{\omega_{pe^+}^2}{\omega(\omega-\omega_{ce^+})}-\frac{\omega_{pi}^2}{\omega(\omega-\omega_{ci})}}\right.\\ &\quad\left.-\sqrt{1-\frac{\omega_{pe}^2}{\omega(\omega+\omega_{ce})}-\frac{\omega_{pe^+}^2}{\omega(\omega+\omega_{ce^+})}-\frac{\omega_{pi}^2}{\omega(\omega+\omega_{ci})}}\right]\\ &= \frac{\omega}{2c}\left[\sqrt{1-\frac{4\pi e^2}{m_e}\frac{n_e}{\omega}\left(\frac{1}{\omega+\frac{eB}{m_ec}}+\frac{X}{\omega-\frac{eB}{m_ec}}+\frac{1-X}{1836\omega-\frac{eB}{m_ec}}\right)}\right.\\ &\quad\left.-\sqrt{1-\frac{4\pi e^2}{m_e}\frac{n_e}{\omega}\left(\frac{1}{\omega-\frac{eB}{m_ec}}+\frac{X}{\omega+\frac{eB}{m_ec}}+\frac{1-X}{1836\omega+\frac{eB}{m_ec}}\right)}\right]\\ &= \frac{\omega}{2c}\left(\sqrt{1-q_L}-\sqrt{1-q_R}\right), \end{aligned} \tag{16}$$

where q_L represents the second term under the first square root of the second equality and q_R represents the second term under the second square root of the second equality.

Equations (11), (12) and (16) presume a cold plasma and it is instructive to comment on the validity of these expressions for a warm plasma. For the latter, motions of charged particles are influenced by thermal effects in addition to the EM force and to express the current density the solution of Vlasov equation is necessary (e.g. Gurnett & Bhattacharjee 2005, chapter 9). Skilling (1971) studied FR for a warm ion–electron plasma and found that for large frequencies away from resonances, the correction to the electron contribution to FR is small compared to the cold plasma term. However, for a pair plasma in which the electron and positron cold plasma terms cancel exactly, warm plasma correction terms would not cancel exactly and a finite contribution would remain. We ignore these small corrections for present purposes and leave further discussion for future work.

2.3.1 High frequency limit

In the high frequency limit ($\omega \gg \omega_{ps}, \omega_{cs}$), we can approximate equation (16) as

$$\begin{aligned}\frac{\mathrm{d}\phi}{\mathrm{d}z} &\simeq \frac{2\pi e^3}{m_e^2c^2}n_eB(1-X)\\ &\quad\times\left\{\frac{1}{\omega^2-[(eB)/(m_ec)]^2}-\frac{1}{1836^2\omega^2-[(eB)/(m_ec)]^2}\right\}\\ &\sim \frac{2\pi e^3}{m_e^2c^2}n_eB(1-X)\left(\frac{1}{\omega^2}-\frac{1}{1836^2\omega^2}\right). \end{aligned} \tag{17}$$

Using equation (15), then equation (17) is the same as equation (12).

For a pure neutral pair plasma ($X = 1$), the right-hand side of equation (16) (or 17) vanishes. The FR vanishes because the equal mass of positrons and electrons induce the same phase speeds for oppositely handed EM waves. This contrasts the limit of the previous section of a pure neutral (hydrogen) ion–electron plasma ($X = 0$), for which the mass asymmetry leads to unequal phase speeds of the oppositely handed waves and a finite right-hand side of equation (16). In general, for $0 \leq X \leq 1$ with n_e, $B_{\rm ex}$ and source distance fixed, the right-hand side of equation (16) decreases with increasing X. We discuss solutions of equation (16) in the next section.

2.3.2 Resonant (low) frequency regime

Before discussing the astrophysical applications of the low-frequency regime, we emphasize that our general equations (11) and (16) can also be used in the frequency regime including $\omega \sim \omega_{cs}$. This limit is not normally considered in astrophysics but has interesting properties of potential future relevance. We consider only the cold plasma limit and ignore thermal broadening effects for present purposes.

Figs 1(a) and (b) show the low-frequency regime of FRs from equation (16) for two different values of X. The plots show four different types of regions for the parameters used. (1) For $1 < \omega < 10$, $10^3 < \omega < 10^4$ and $10^5 < \omega < 10^6$ Hz where both LH and RH waves propagate and a FR can be measured. (2) There are resonances where $\omega = \omega_{ce} = eB/m_ec = 1.76 \times 10^7\, B$ and $\omega = \omega_{ci} = eB/m_ic = 9571\, B$ at which the FR blows up. The FR would exhibit sharp resonance features near the singular points, allowing the B field to be inferred in principle. However, for applications to extended jets of AGN and larger scale systems, these resonant frequencies are generally small compared to the relevant

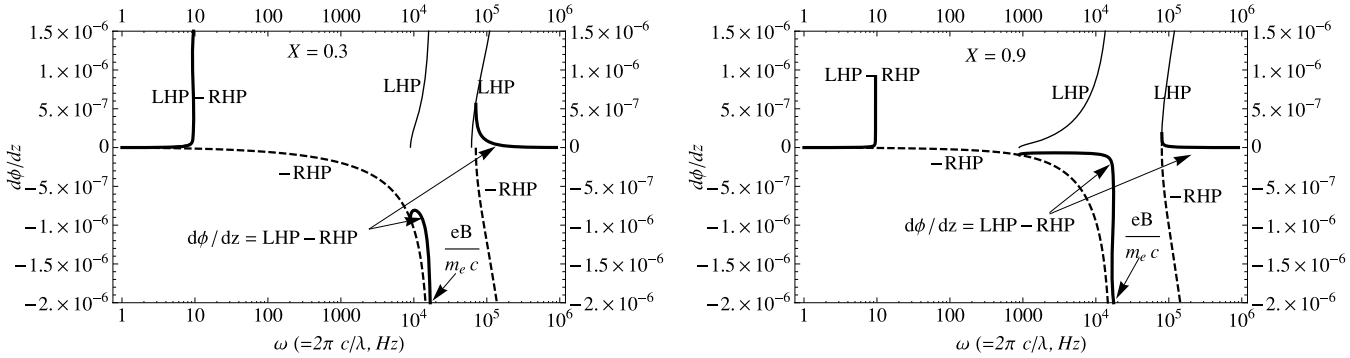

(a) FR angle at X=0.3 (b) FR angle at X=0.9

Figure 1. The FR angle per cm in low-frequency regime for (a) $X = 0.3$ and (b) $X = 0.9$. The plots are from the exact expression FR equation (16) with $B = 1\,\mathrm{mG}$ and $n_e = 1\,\mathrm{cm}^{-3}$ to exemplify four different types of regions. In both panels, the thin solid lines indicate the rotation for the LHP wave and the dashed lines indicate the rotation for the RHP waves. The thick solid lines are the sum of the two at frequencies where both propagate. Note that there is a region $10^4 < \omega < 10^5$ Hz where both LHP and RHP waves are evanescent (do not propagate), and a region $10 < \omega < 10^3$ Hz where only the RHP propagates. See Section 2.3.2 for more discussion of the figure.

∼GHz frequencies. (3) For $10^4 < \omega < 10^5$ Hz, FR does not exist because both LH and RH waves are evanescent (both LHP and RHP waves become imaginary and do not propagate). (4) For $10 < \omega < 1000$ Hz, the LHP is evanescent. In that case, the real part is a RH circularly polarized wave. Unless observations of the plane of polarization at two different frequencies could be made with a time resolution much less than the period of the rotating electric field vector of the wave, information about the source field, composition or density cannot be extracted as in the case when both RHP and LHP propagate to make a linearly polarized wave. For the latter case, the observer measures the plane of polarization at two different wavelengths and can subtract the two measurements to obtain RM. This requires that the initial plane of polarization of the waves at the two different wavelengths is the same, and the difference arises only over propagating through the source. In contrast, the initial plane of polarization of the circularly polarized waves changes on a time-scale equal to the period of the wave. Unless this is much longer than the time resolution of the detector, the initial plane of polarization for the circularly polarized waves is indeterminate and the RM cannot be inferred.

3 ASTROPHYSICAL IMPLICATIONS

We now consider the astrophysical implications of our FR calculations and focus on the high frequency limit.

3.1 General implications of plasma composition

Figs 2 and 3 show solutions to the exact expression equation (16) and the approximation equation (17) for n_e, B and X at fixed values of RMs ($2600\,\mathrm{rad\,m^{-2}}$ in Fig. 2 and $1000\,\mathrm{rad\,m^{-2}}$ in Fig. 3). The RMs were converted into rotation angles for cm scale at $\lambda = 1.35\,\mathrm{cm}(22.2\,\mathrm{GHz})$. The FR in Fig. 2 corresponds to 3.63 pc (749 Mpc × 0.5 mas, C1 region) from the core of AGN jet 3C 273 from Zavala & Taylor (2001). From synchrotron emission, Savolainen et al. (2006) calculated the total magnetic field to be ($B \sim 0.06\,\mathrm{G}$) in this region. If this were the line-of-sight field, Fig. 2(b) shows that $n_e \geq 0.05\,\mathrm{cm}^{-3}$ for RM ($2600\,\mathrm{rad\,m^{-2}}$), the minimum n_e occurring at $X = 0$. Fig. 3(c) shows a complementary example for values appropriate for a typical X-ray cluster (Jaffe 1980) with $n_e \sim 0.003\,\mathrm{cm}^{-3}$ and RM ∼$1000\,\mathrm{rad\,m^{-2}}$. The standard assumption that $X = 0$ for a known distance leads directly to the inference that $B \sim 1\,\mu\mathrm{G}$ (Jaffe 1980). But for any $X < 1$, Fig. 3(b) for example, shows how much stronger the field could be.

For fixed values of RM, Figs 2(a) and 3(a) show that n_e and B behave oppositely for each value of X: as n_e increases (decreases), B decreases (increases). These trends reflect that the RM is roughly proportional to the field and the density. Figs 2(a), (b) and 3(a), (b) show that as X increases (decreases), B and n_e increase (decrease), respectively. These trends result because an increasing X means a higher fraction of pair plasma. The latter contributes zero FR so that a higher B or n_e is needed for a fixed RM. Figs 2(c) and 3(c) reflect these same trends.

In all panels, the lines resulting from equation (16) are indistinguishable from those obtained using equation (17) for the parameters used, highlighting the efficacy of the latter. Figs 3(a)–(c) are very similar to Figs 2(a)–(c) as only the vertical axis scales are different due to the different RM choices. Overall, the figures show how an unknown plasma composition X implies degeneracies in the values n_e and B, or complementarily, how independent measures of n_e and B can be combined with an RM to constrain X. We emphasize that the path length l [that relates RM to $\mathrm{d}\phi/\mathrm{d}z$ via $\int_0^l (\mathrm{d}\phi/\mathrm{d}z)\,\mathrm{d}z$] may itself be a uncertain quantity. In making our plots, we used the values for l and RM given by the specific authors from which the data were taken.

3.2 Further discussion of applications

If the RM and two of the three quantities n_e, X and B are independently known, the FR equation is exactly determined. However, even if only one variable and RM are known, the other variables can be constrained.

There have been efforts to interpret the RM with a subset of independently measured variables n_e, B and T. For example, Zavala & Taylor (2002) calculated the B field in M87 using the RM and an independently determined n_e. For $\mathrm{RM} = -4000\,\mathrm{rad\,m^{-2}}$, equation (13) was used to get B∼15 μG, but $X = 0$ was assumed. We can revisit the interpretation of the measured RM without assuming $X = 0$ a priori. As seen in Fig. 4(a), the cross point of B∼15 μG and $\mathrm{RM} = -4000\,\mathrm{rad\,m^{-2}}$ with $n_e = 1100\,\mathrm{cm}^{-3}$ (dashed line) is $X = 0$. In contrast, if we suppose that $B = 200\,\mu\mathrm{G}$, which corresponds to the thermal equipartition condition when $T \sim 10^4$ K

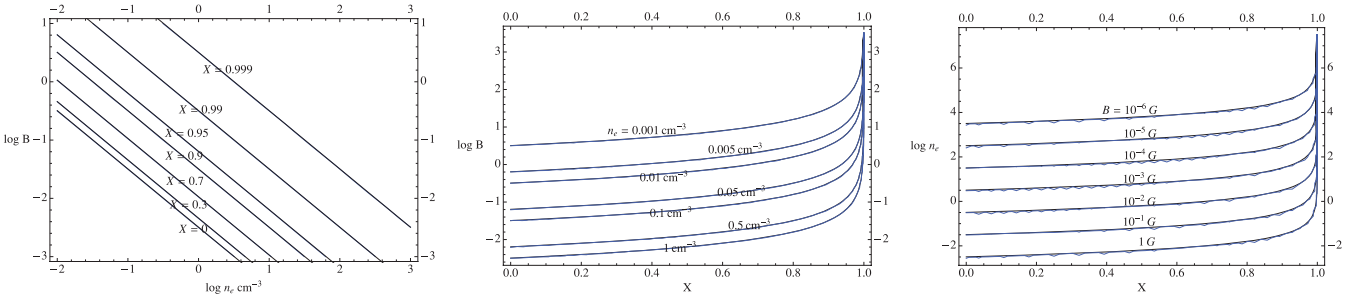

(a) log B vs log n_e (b) log B vs X (c) log n_e vs X

Figure 2. Plots of n_e, B and X. All panels use a fixed RM $\sim 2600\,\mathrm{rad\,m^{-2}}$ in Zavala & Taylor (2001) (their fig. 3). The line-of-sight B field is estimated at $\sim$0.5 mas ($\sim$3.63 pc) from the core. All of the plots were made using both equation (16) and equation (17) with $\lambda = 1.35$ cm (22.2 GHz). The plots of each equation were overlapped highlighting the efficacy of the approximate equation. The original observation frequency is 8 GHz but any frequency gives the same RM.

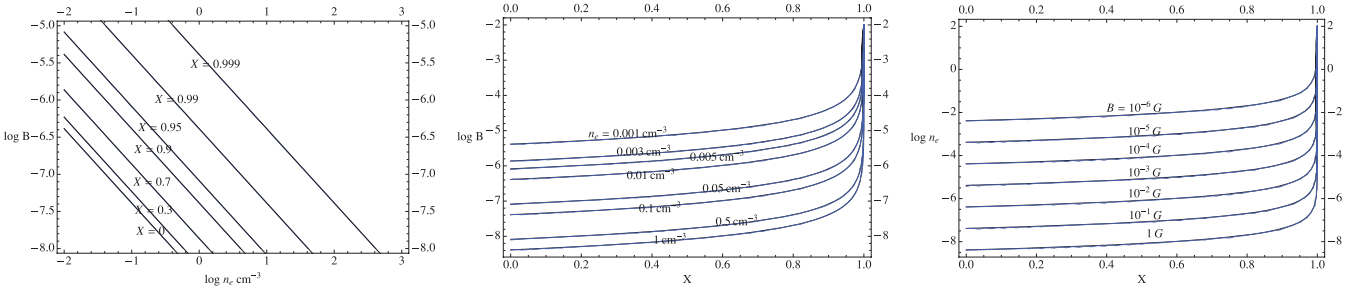

(a) log B vs log n_e (b) log B vs X (c) log n_e vs X

Figure 3. Same as Fig. 2, but using RM $\sim 1000\,\mathrm{rad\,m^{-2}}$ with path length $l = 300$ kpc, in an X-ray cluster core (Jaffe 1980) with $\lambda = 1.3$ cm (22.2 GHz). Again both equations (16) and (17) were used for the plots.

($n_e k_B T = B^2/8\pi$, where B is the mean line-of-sight field that causes FR, e.g. Gabuzda, Pushkarev & Garnich 2008), different X values result: for RM = 9000 rad m^{-2} and -4000 rad m^{-2}, the X values are 0.83 and 0.92, respectively. The corresponding n_{e^+} values are 913 and 1012 cm^{-3}. If instead magnetic pressure dominates (e.g. dominant $\beta \equiv P_g/P_B = 8\pi\, n_e k_B T/B^2 < 1$), then X increases as shown in Fig. 4.

As another set of examples showing the degeneracy between B and X, we consider the independently measured RM, n_e, B and T for clusters A400, A1795 and A2199 (Eilek & Owen 2002) which respectively include radio sources 3C75, 4C46.42 and 3C338 to obtain Fig. 4(b). B is also the mean line-of-sight field but we note that the definition of the magnetic pressure ($P_B = 3 < B_\parallel >^2/8\pi$) is different from that of Zavala & Taylor (2002). We have taken

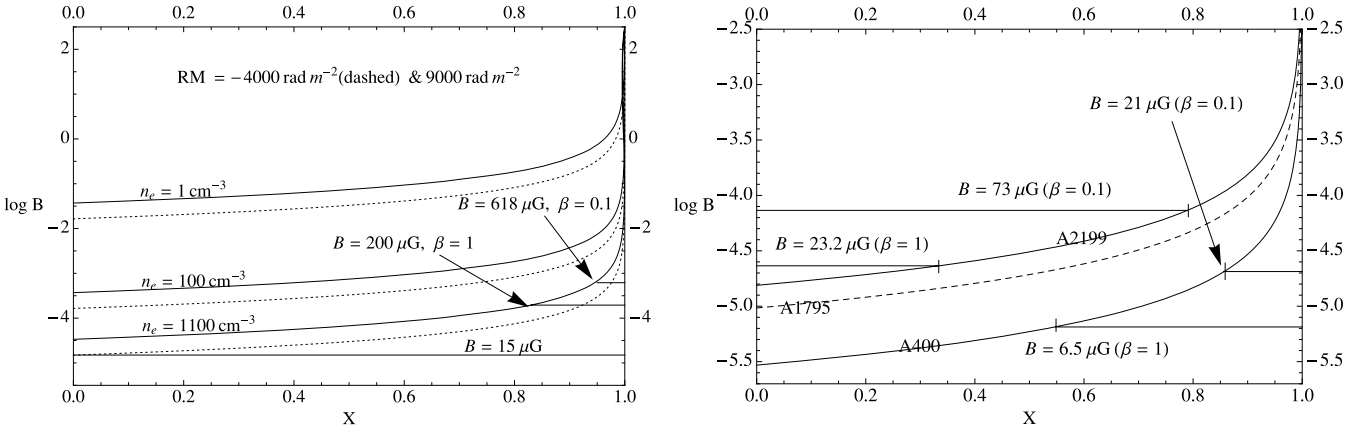

(a) log B vs X for M87 (Zavala & Taylor 2002) (b) log B vs X for Abell clusters (Eilek & Owen 2002)

Figure 4. These log B versus X plots were made using RM, B, n_e and T from Zavala & Taylor (2002) and Eilek & Owen (2002). The rotation angle for (a) was converted from the RM -4000 rad m^{-2} (dashed line) and 9000 rad m^{-2} (solid line) at $\lambda = 1.35$ cm (22.2 GHz). For (b), each data point for RM (50, 1500, 750 rad m^2); n_e (0.0021, 0.064, 0.02 cm^{-3}) and T (1.5, 5.1, 1.2 keV) where the values in parentheses are for A400, A1795 and A2199, respectively, were also plotted for 22.2 GHz. The values of β correspond to the particular cluster which the separate lines of B intersect, explaining why different values of the field correspond to the same $\beta = 0.1$ for A400 and A2199.

this into account when interpreting their respective data. There, instead of assuming $X = 0$, as is normally done to obtain the B, we chose selected field strengths (straight lines on the plot) and identify the constraints this places on X by where these lines intersect with the curves. For example, for A400, if magnetic and thermal pressures were in equipartition ($\beta = 1$), the data would imply $X = 0.55$ (here $n_e = 0.0021\,\mathrm{cm}^{-3}, n_{e^+} = 1.155 \times 10^{-3}\,\mathrm{cm}^{-3}, n_i = 9.45 \times 10^{-4}\,\mathrm{cm}^{-3}$). However, if magnetic pressures were dominant (e.g. $\beta = 0.1$), then $X = 0.86 (n_e = 0.0021\,\mathrm{cm}^{-3}, n_{e^+} = 1.806 \times 10^{-3}\,\mathrm{cm}^{-3}, n_i = 2.94 \times 10^{-4}\,\mathrm{cm}^{-3})$. The extent to which X differs form zero in clusters could depend on how close to a radio source core the RM is measured as one would indeed expect $X = 0$ far away from radio jets. As better spatial coverage of both FR and synchrotron constraints become available for jets, the use of plots such as those of Figs 2 and 3 become more powerful.

4 CONCLUSIONS

We have derived a generalized expression of FR for a plasma of arbitrary composition that is valid for arbitrary radiation frequencies. This includes low frequencies where there can be resonances at specific frequencies or a range of frequencies where either one or both the LHP and RHP waves are evanescent.

Focusing then on the higher frequency regime where both LHP and RHP propagate in the specific case of a neutral plasma containing electrons, positrons and ions, we show how a given value of RM implies degeneracies in the magnetic field strength and electron number density for different positron to electron number density ratios. Positrons contribute an equal magnitude but oppositely signed RM to electrons. Thus for a given RM, a larger value of X would imply a field strength and or electron density in excess of that inferred for $X = 0$. Complementarily, as the ratio of positrons to electrons X increases from 0 to 1, the RM decreases for a given line-of-sight magnetic field and density.

While $X = 0$ is often assumed for astrophysical plasmas, this assumption is not necessarily valid for jets and magnetospheres of black holes and neutron stars, where in fact it is of interest to independently determine X. We have shown quantitatively the degeneracies in the space of parameters n_e, X and B, and how they can be constrained. In principle, if independent data on B and n_e can be obtained, then a given RM measurement can be used to obtain X. The pursuit of X has been particularly elusive in the context of AGN jets and we hope that the calculations and strategy herein provide a tool toward better constraining the composition and help to motivate the pursuit of more data.

ACKNOWLEDGMENTS

KP acknowledges a Horton Graduate Fellowship from the Laboratory for Laser Energetics at the University of Rochester. EGB acknowledges support from NSF grants AST-0406799 AST-0807363, and NASA grant ATP04-0000-0016. We also thank D. Gabudza for comments.

REFERENCES

Asada K., Inoue M., Uchida Y., Kameno S., Fujisawa K., Iguchi S., Mutoh M., 2002, PASJ, 54, L39
Asada K., Inoue M., Kameno S., Nagai H., 2008, ApJ, 675, 79
Ashok D., 2004, Lectures on Electromagnetism, 1st edn. Rinton Press, Paramus, p. 389
Attridge J. M., Wardle J. F. C., Homan D. C., 2005, ApJ, 633, L85
Blandford R. D., Znajek R. L., 1977, MNRAS, 179, 433
Celotti A., Fabian A. C., 1993, MNRAS, 264, 228
Eilek J. A., Owen F. N., 2002, ApJ, 567, 202
Gabuzda D. C., Pushkarev A. B., Garnich N. N., 2001, MNRAS, 327, 1
Ghisellini G., 2008, Int. J. Modern Phys. D, 17, 1491
Gurnett D. A., Bhattacharjee A., 2005, Introduction to Plasma Physics. Cambridge Univ. Press, Cambridge, p. 94
Hall J. O., Shukla P. K., 2005, Phys. Plasma, 12, 084507
Han J. L., Manchester R. N., Lyne A. G., Qiao G. J., van Straten W., 2006, ApJ, 642, 868
Hubbard A., Blackman E. G., 2006, MNRAS, 371, 1717
Jaffe W., 1980, ApJ. 241, 925
Kim K.-T., Kronberg P. P., Dewdney P. E., Landecker T. L., 1990, ApJ, 355, 29
Li H., Lapenta G., Finn J. M., Li S., Colgate S. A., 2006, ApJ, 643, 92
Livio M., Ogilvie G. I., Pringle J. E., 1999, ApJ, 512, 100
Michel F. C., 1982, Rev. Mod. Phys., 54, 1
Reynolds C. S., Fabian A. C., Celotti A., Rees M. J., 1996b, MNRAS, 283, 873
Savolainen T., Wiik K., Valtaoja E., Tornikoski M., 2006, A&A, 446, 71
Skilling J., 1971, Phys. Fluids, 14, 2523
Zavala R. T., Taylor G. B., 2001, ApJ, 550, L147
Zavala R. T., Taylor G. B., 2002, ApJ, 566, L9
Zavala R. T., Taylor G. B., 2005, ApJ, 626, L73

This paper has been typeset from a TEX/LATEX file prepared by the author.